Data in brief 28 (2020) 104883

Contents lists available at ScienceDirect

Data in brief

journal homepage: www.elsevier.com/locate/dib

Data Article

Experimental data on synthesis and characterization of chiral dinuclear manganese (II-II) compounds as biomimetic models of the active center of catalase

Yenny Ávila-Torres [a, *], Jorge Acosta [a], Lázaro Huerta [b], Alfredo Toscano [c], Felipe J. González [d], Norah Barba Behrens [c]

[a] Grupo de Investigación QUIBIO, Facultad de Ciencias Básicas, Universidad Santiago de Cali, Santiago de Cali, Pampalinda, Colombia
[b] Instituto de Investigaciones en Materiales, Universidad Nacional Autónoma de México, C.U., Coyoacán, México D.F., 04510, Mexico
[c] Instituto de Química, Universidad Nacional Autónoma de México, C.U., Coyoacán, México D.F., 04510, Mexico
[d] Departamento de Química, Cinvestav México, AP 14-740, CP 07000, México DF, Mexico

ARTICLE INFO

Article history:
Received 24 August 2019
Received in revised form 18 November 2019
Accepted 19 November 2019
Available online 2 December 2019

Keywords:
Manganese-catalases
Electronic properties
Magnetic properties
Functional structure
Chiral ligands

ABSTRACT

Dinuclear manganese (II– III) compounds, which are potential models of the active center of catalase, were synthetized. This type of metalloenzymes presents biological importance due to three factors: they are redox catalyst centres, they are able to carry out hydrolytic reactions and they participate in activated processes via Lewis acids. Structurally, their active centre is composed by dinuclear manganese compounds, linked to nitrogen and oxygen donor atoms. An octahedral geometry around the metal ions were found, with acetate, hydroxy and aquo ligands; which can work as molecule bridges between them. The acid medium favours the electronic transfer between Mn^{3+} - Mn^{2+} as redox centre at 1.559 V and the consequent oxidation of hydrogen peroxide or organic molecules. The work also reports the data of two chiral novel compounds, $[Mn_2(S,S(+)Hcpse)_4(NaClO_4)_2(NaOH)(CH_4O)]_n\cdot[(C_2H_6O)_2]_n\cdot[(CH_4O)_2]_n$ and its respective enantioisomer, in which μ-oxo being as bridge metal centre. The X-ray structural was obtained as well as the optical and magnetic properties using Circular Dichroism,

* Corresponding author.
E-mail address: yennytorres@usc.edu.co (Y. Ávila-Torres).

https://doi.org/10.1016/j.dib.2019.104883

Electronic Paramagnetic Resonance, Magnetic Susceptibility and X-ray photoelectron spectroscopy.

Specifications Table

Subject	Inorganic Chemistry
Specific subject area	Bioinorganic chemistry, Science Materials
Type of data	Tables and Figures
How data were acquired	X-ray crystallographic study (DRX) Valence metal centres (XPS) Chiral activity (Circular dichroism) Electrochemical study (Voltammetry cyclic) Magnetic properties (Susceptibility magnetic at variable temperature)
Data format	Raw
Parameters for data collection	The data shown in this article are obtained from the methanol synthesis of the tridentate ligand - N acetyl pseudoephedrine with manganese (II), as structural biomimetic models of catalase and peroxidases. Likewise, its structural (X- ray crystal), optical (CD spectra), electronic (electrochemical analyses) and magnetic (EPR and susceptibility magnetic) characterization was carried out.
Description of data collection	The data collection was obtained of the synthesis and crystal structures of two manganese (II) complexes containing chiral aminoalcohols (*R,R* (−)H_2cpse) and (*S,S* (+) H_2cpse). The 1:1 reaction between Mn(CH_3COOH)·$4H_2O$ and ligands, followed by the addition of NaOH and $NaClO_4$ in methanol afforded the polymeric compounds. In solution, a change of the oxidation state of the manganese ion was observed using voltammetry cyclic and circular dichroism in comparison with XPS, which will serve to understand the electronic exchange in dissolution when using these models as catalase or peroxidases.
Data source location	Institution: Universidad Santiago de Cali City/Town/Region: Santiago de Cali Country: Colombia
Data accessibility	The data are found only in this article.

Value of the Data

- The new chiral ligands with manganese (II) reported are new interesting biomimetic models of metalloenzymes such as catalases. The characterization of these synthetic models emulating biological processes allows the design of new structures and to test experimentally the models reported here.
- Data can be used to compare the stability of the biomimetic compounds in solid state and in solution.
- Data are useful in the study of the mechanism of chiral compounds action in oxidases, which oxidize organic molecules and substrates such as hydrogen peroxide with several potential applications in water treatment and decorating dyes among others.
- These data show molecules that are related to enantioselective synthesis, where the metallic centre and the chiral ligand provide important optical properties that can affect intermolecular interactions in processes associated with metalloenzymes, such as: manganese peroxidases and catalase manganese.

1. Data

The data files of $[Mn_2(S,S(+)Hcpse)_4(NaClO_4)_2(NaOH)(CH_4O)]_n\cdot[(C_2H_6O)_2]_n\cdot[(CH_4O)_2]_n$ and its respective isomer showed that in solid state the asymmetric unit is composed by a dinuclear manganese (II) entity, Tables 1–3; likewise Hydrogen Bonds (°) and distances (Å) in Table 4 and Figs. 1–3. These structures showed similar coordination to metal center, as in metalloenzimes catalases. This was confirmed by X-ray crystal analysis, Fig. 4; spectra XPS, Fig. 5 and Fig. 6; and their antiferromagnetic properties, Fig. 7. Furthemore, in solution the electrochemical characterization indicated that the

Table 1
Crystal data and structure refinement for $[Mn_2(S,S(+)Hcpse)_4(NaClO_4)_2(NaOH)(CH_4O)]_n\cdot[(C_2H_6O)_2]_n\cdot[(CH_4O)_2]_n$.

Chemical formula (Sum)	$C_{51}H_{79}Cl_2Mn_2N_4Na_3O_{25}$
Formula weight (Sum) (g mol^{-1})	1397.93
Crystal colour	dark purple
Crystal system	Monoclinic
Space group	C2
Unit cell dimensions	
a (Å)	21.5749 (8)
b (Å)	18.8865 (5)
c (Å)	17.6692 (6)
α (°)	90.0
β (°)	113.624 (4)
γ (°)	90.0
V ($Å^3$)	6589.4 (4)
Z	4
$^{D}calc$ (g/cm3)	1.409
F (000)	2920
Temp (K)	130
θ range (°)	3.3855−29.4984
Index range	$-27 \leq h \leq 24$ $-25 \leq k \leq 24$ $-24 \leq l \leq 21$
Reflections measured	27019
Independent reflections	15140
Reflections *[I > 2σ(I)]*	9048
R_{int}	0.0660[a]
R	0.0621
R_w	0.1363
S	0.928

[a] $Rint = \sum\left|F_o^2 - \langle F_o^2\rangle\right| / \sum F_o^2$, $R_1 = \sum||F_o| - |F_c|| / \sum|F_o|$, $wR_2 = [\sum w(F_o^2 - F_c^2)/\sum w(F_o^2)^2]^{1/2}$

Table 2
Selected bond distances (Å) of the *$[Mn_2(S,S(+)Hcpse)_4(NaClO_4)_2(NaOH)(CH_4O)]_n[(C_2H_6O)_2]_n\cdot[(CH_4O)_2]_n$*.

Mn1−O1	1.868 (4)
Mn1−O2	1.848 (5)
Mn1−O5	2.127 (5)
Mn1−O6	2.113 (4)
Mn1−N1	2.159 (5)
Mn1−N2	2.163 (6)
Mn2−O3	1.863 (4)
Mn2−O4	1.862 (5)
Mn2−O7	2.126 (4)
Mn2−O8	2.065 (5)
Mn2−N3	2.168 (5)
Mn2−N4	2.206 (5)
Mn1−Na3	3.384 (3)
Mn2−$Na2^1$	3.611 (3)
Na1−Na2	3.339 (4)
Na2−Na3	3.581 (4)
Na3−Na4	3.606 (3)
Na1−O10	2.361 (4)
Na1−O12	2.469 (6)
Na1−O13	2.464 (9)
Na2−O7	2.737 (6)
Na2−O8	2.330 (5)
Na2−O10	2.340 (5)
Na2−O12	2.355 (6)
Na2−O21	2.341 (6)

Na2−O22	2.454 (6)
Na3−O5	2.343 (6)
Na3−O6	2.360 (5)
Na3−O7	3.048 (6)
Na3−O17	2.397 (10)
Na3−O11	2.271 (7)
Na3−O21	2.325 (7)
Na4−O9	2.395 (7)
Na4−O17	2.927 (15)
Na4−O11^{I}	2.319 (5)
Na4−O11^{II}	2.319 (5)
Na4−O9^{III}	2.395 (7)
Na4−O17^{III}	2.927 (15)

Table 3
Selected angles (°) for *[Mn$_2$(S,S(+)Hcpse)$_4$ (NaClO$_4$)$_2$(NaOH)(CH$_4$O)]$_n$[(C$_2$H$_6$O)$_2$]$_n$·[(CH$_4$O)$_2$]$_n$* compound.

O2−Mn1−O1	172.3 (2)
O2−Mn1−O6	96.5 (2)
O1−Mn1−O6	90.4 (2)
O2−Mn1−O5	88.0 (2)
O1−Mn1−O5	96.9 (2)
O6−Mn1−O5	79.6 (2)
O2−Mn1−N1	92.0 (2)
O1−Mn1−N1	83.2 (2)
O6−Mn1−N1	154.7 (2)
O5−Mn1−N1	76.9 (2)
O2−Mn1−N2	83.2 (2)
O1−Mn1−N2	94.8 (2)
O6−Mn1−N2	77.4 (2)
O5−Mn1−N2	154.2 (2)
N1−Mn1−N2	127.4 (2)
O4−Mn2−O3	170.1 (2)
O4−Mn2−O8	93.0 (2)
O3−Mn2−O8	95.9 (2)
O4−Mn2−O7	94.4 (2)
O3−Mn2−O7	91.6 (2)
O8−Mn2−O7	79.6 (2)
O4−Mn2−N3	89.9 (2)
O3−Mn2−N3	83.3 (2)
O8−Mn2−N3	159.6 (2)
O7−Mn2−N3	80.1 (2)
O4−Mn2−N4	82.9 (2)
O3−Mn2−N4	94.4 (2)
O8−Mn2−N4	79.0 (2)
O7−Mn2−N4	158.2 (2)
N3−Mn2−N4	121.4 (2)
O10^{I}−Na1−O10	179.4 (3)
O10^{I}−Na1−O13	81.0 (3)
O10−Na1−O13	98.5 (3)
O10^{I}−Na1−O13^{I}	98.5 (3)
O10−Na1−O13^{I}	81.0 (3)
O13−Na1−O13^{I}	74.3 (6)
O10^{I}−Na1−O12	103.3 (2)
O10−Na1−O12	77.2 (2)
O13−Na1−O12	105.2 (3)
O13^{I}−Na1−O12	157.9 (3)
O10^{I}−Na1−O12^{I}	77.2 (2)
O10−Na1−O12^{I}	103.3 (2)
O13−Na1−O12^{I}	157.9 (3)
O13^{I}−Na1−O12^{I}	105.2 (3)
O12−Na1−O12^{I}	83.6 (3)
O8^{I}−Na2−O10	89.3 (2)
O8^{I}−Na2−O21	152.1 (2)

O10—Na2—O21	93.1 (2)
O8^{I}—Na2—O12	105.6 (2)
O10—Na2—O12	79.9 (2)
O21—Na2—O12	102.1 (2)
O8^{I}—Na2—O22	78.0 (2)
O10—Na2—O22	157.6 (2)
O21—Na2—O22	106.7 (2)
O12—Na2—O22	85.8 (2)
O8^{I}—Na2—O7^{I}	63.3 (2)
O10—Na2—O7^{I}	94.6 (2)
O21—Na2—O7^{I}	88.8 (2)
O12—Na2—O7^{I}	168.0 (2)
O22—Na2—O7^{I}	96.0 (2)
O11^{I}—Na3—O21	123.3 (2)
O11^{I}—Na3—O5	88.9 (2)
O21—Na3—O5	146.5 (2)
O11^{I}—Na3—O6	105.5 (2)
O21—Na3—O6	90.1 (2)
O5—Na3—O6	70.5 (2)
O11^{I}—Na3—O17	82.3 (4)
O21—Na3—O17	109.5 (3)
O5—Na3—O17	81.5 (3)
O6—Na3—O17	150.5 (3)
O11^{I}—Na4—O11^{II}	162.9 (4)
O11^{I}—Na4—O9^{III}	81.5 (2)
O11^{II}—Na4—O9^{III}	112.4 (2)
O11^{I}—Na4—O9	112.4 (2)
O11^{II}—Na4—O9	81.5 (2)
O9^{III}—Na4—O9	77.2 (4)
O11^{I}—Na4—O17^{III}	105.4 (2)
O11^{II}—Na4—O17^{III}	70.7 (2)
O9^{III}—Na4—O17^{III}	74.4 (3)
O9—Na4—O17^{III}	127.9 (3)
O11^{I}—Na4—O17	70.7 (2)
O11^{II}—Na4—O17	105.4 (2)
O9^{III}—Na4—O17	127.9 (3)
O9—Na4—O17	74.3 (3)
O17^{III}—Na4—O17	154.5 (5)

Symmetry transformations used to generate equivalent atoms: ^{I} -x+1,y,-z+1, ^{II} x,y,z-1, ^{III} -x+1,y,-z, ^{IV} x,y,z+1, ^{V} -x+1/2,y+1/2,-z, ^{VI} -x+1/2,y-1/2,-z+1.

Table 4
Hydrogen Bonds (°) and distances (Å) of *[Mn$_2$(S,S(+)Hcpse)$_4$(NaClO$_4$)$_2$(NaOH)(CH$_4$O)]$_n$[(C$_2$H$_6$O)$_2$]$_n$·[(CH$_4$O)$_2$]$_n$*.

D-H … A	d (D-H) (Å)	d ˋÅ)	<(DHA) (°)
O1—H1A … O23		1.78	166.3
O3—H3 … O22^{I}		1.84	178.5
O21—H21 … O20	0.85	2.34	122.7
O21—H21 … O22C	0.85	2.14	139.6
O23—H23C … O21	0.84	2.26	127.6
O24—H24C … O7^{I}	0.85	2.66	179.4
O25—H25C … O24^{I}	0.85	1.97	179.6
O25—H25D … O10^{I}	0.85	1.89	179.6
C6—H6 … O15^{I}		1.00	136.1
C17—H17C … O19^{II}	0.98	2.65	167.4
C19—H19B … O14^{III}	0.98	2.61	164.7
C26—H26 … O18^{II}	0.98	2.54	165.7
C45—H45B … O20^{II}	2.46	3.42	166.1
C37—H37 … Cg1^{III}	0.98	2.84	145
C48—H48A … Cg2^{III}	0.98	2.83	128

Symmetry transformations used to generate equivalent atoms: ^{I}-x+1,y,-z+1, ^{II} -x+1/2,y+1/2,-z, ^{III} - x+1/2,y-1/2,-z+1. Cg1: C21→C26; Cg2: C27→C32.

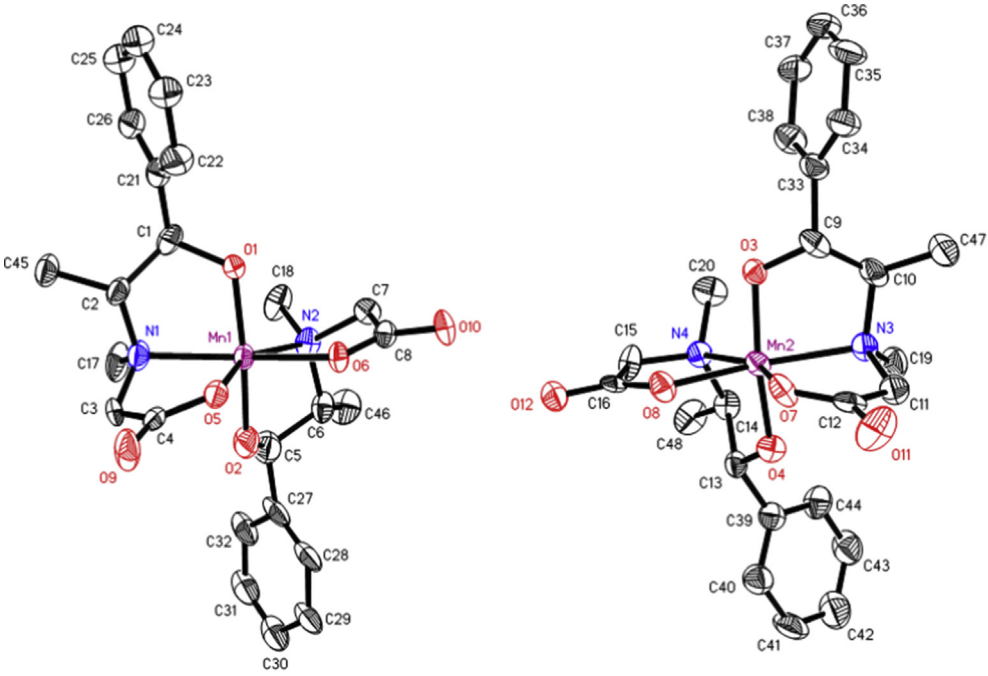

Fig. 1. Ortep representation of the $[Mn_2(S,S(+)Hcpse)_4(NaClO_4)_2(NaOH)(CH_4O)]_n[(C_2H_6O)_2]_n{\cdot}[(CH_4O)_2]_n$ compound.

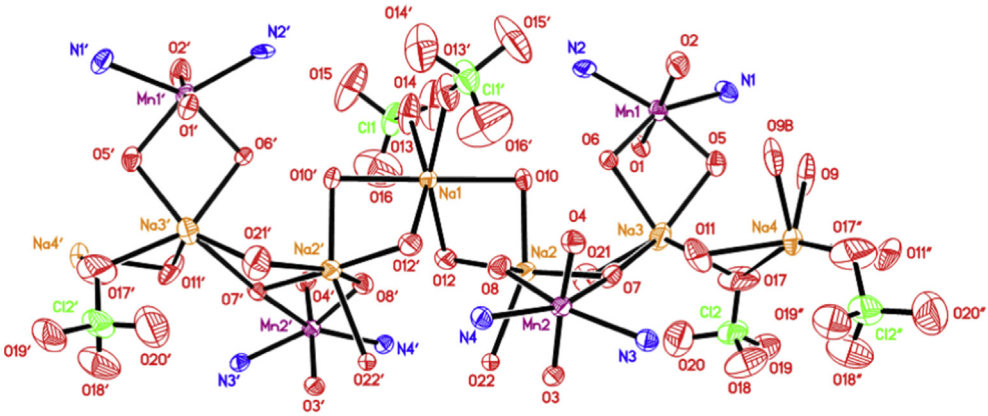

Fig. 2. Polymeric structure for $[Mn_2(S,S(+)Hcpse)_4(NaClO_4)_2(NaOH)(CH_4O)]_n[(C_2H_6O)_2]_n{\cdot}[(CH_4O)_2]_n$ compound.

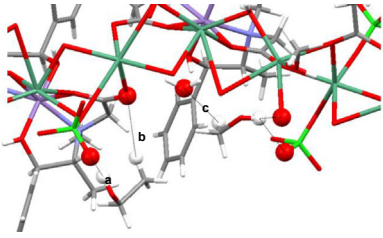

a. 1.634 Å, 126.17°

b. 2.711 Å, 109.96°

c. 2.119 Å, 102.73°

Fig. 3. Intermolecular interactions for $[Mn_2(S,S(+)Hcpse)_4(NaClO_4)_2(NaOH)(CH_4O)]_n[(C_2H_6O)_2]_n{\cdot}[(CH_4O)_2]_n$.

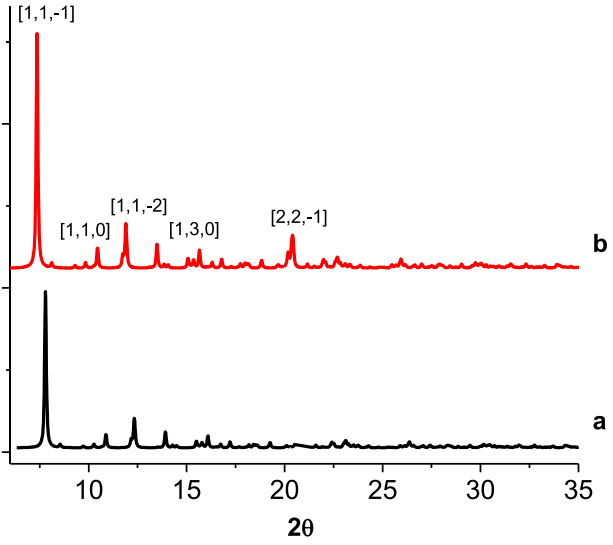

Fig. 4. X-ray powder diffraction for: *a)* $[Mn_2(S,S(+)Hcpse)_4(NaClO_4)_2(NaOH)(CH_4O)]_n\cdot[(C_2H_6O)_2]_n\cdot[(CH_4O)_2]_n$, *b)* $[Mn_2(R,R(-)Hcpse)_4(NaClO_4)_2(NaOH)(CH_4O)]_n\cdot[(C_2H_6O)_2]_n\cdot[(CH_4O)_2]_n$.

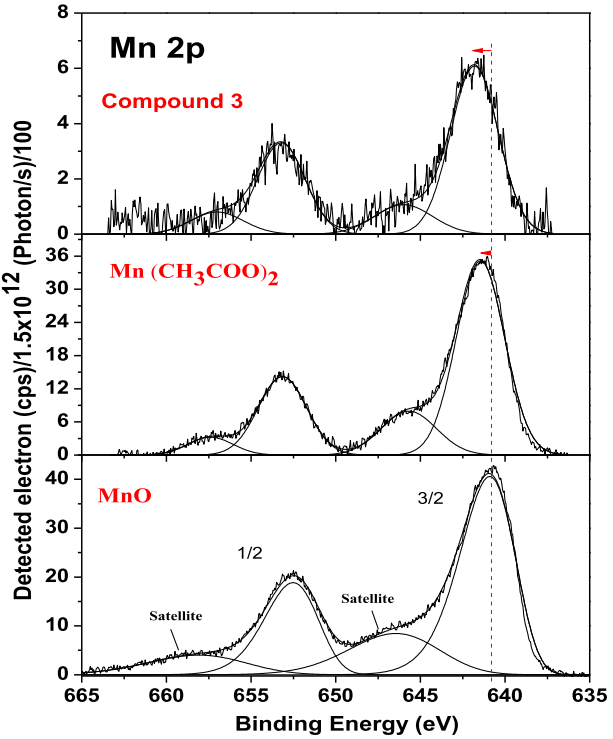

Fig. 5. XPS spectra of Mn 2p core level of MnO, $Mn(CH_3COO)_2$ and compound $[Mn_2(S,S(+)Hcpse)_4(NaClO_4)_2(NaOH)(CH_4O)]_n\cdot[(C_2H_6O)_2]_n\cdot[(CH_4O)_2]_n$.

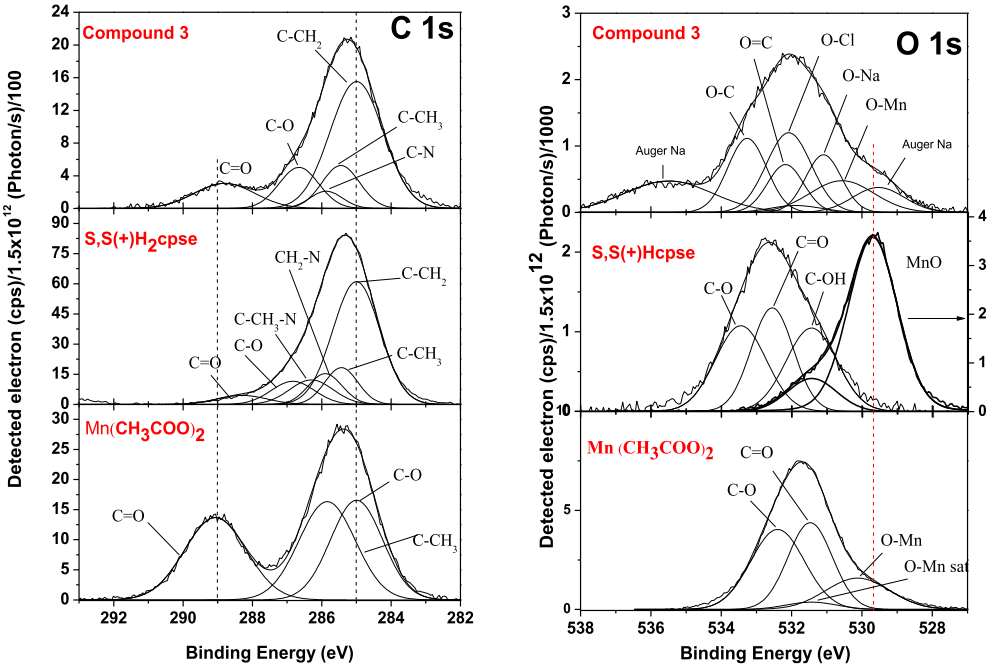

Fig. 6. The high resolution XPS spectra of C 1s, and O 1s core level. XPS data of $Mn(CH_3COO)_2$, (S,S (+)H_2cpse), and compound $[Mn_2(S,S(+)Hcpse)_4(NaClO_4)_2(NaOH)(CH_4O)]_n{\cdot}[(C_2H_6O)_2]_n{\cdot}[(CH_4O)_2]_n$.

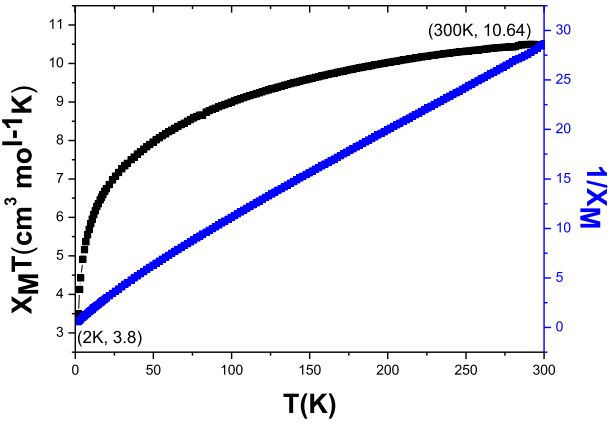

Fig. 7. Temperature dependence of $\chi_M T$ vs. T for a) $[Mn_2(S,S(+)Hcpse)_4(NaClO_4)_2(NaOH)(CH_3OH)]_n{\cdot}[(C_2H_6O)_2]_n{\cdot}[(CH_4O)_2]_n$.

oxidation state for metal ions involved a slow electron transfer step followed by chemical reaction, which most probably corresponds to a bond breaking step, Figs. 8–10. Likewise, the presence of only a one-electron oxidation peak implies that the manganese possesses a single oxidation state in this complex, with dissociation of the dinuclear compound into a monomer, where the manganese ions presented oxidation (III) as valence state, in agreement with the CD, Fig. 11; and EPR measurements, Fig. 12; [1–7].

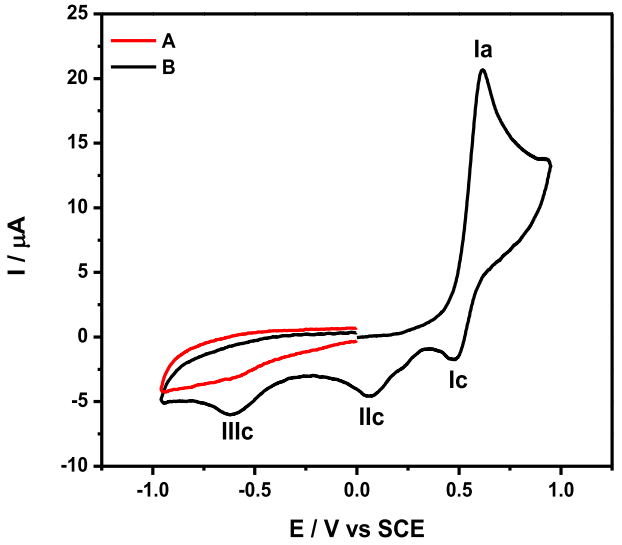

Fig. 8. Cyclic voltammetry for **3**–1 mM, on glassy carbon electrode (ϕ = 3 mm), in acetonitrile containing *n*-Bu_4NPF_6 0.1 M. a) positive direction starting scan, b) negative direction starting scan. Scan rate: 0.1 V s^{-1}.

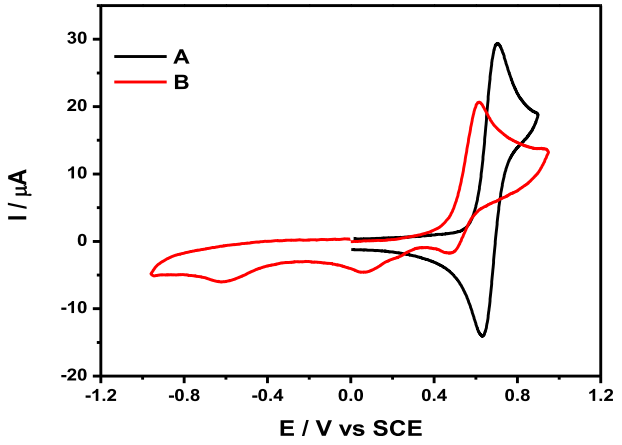

Fig. 9. Comparison of the current due to the oxidation of ferrocenecarboxaldehyde 1 mM (A) with that for compound **3** ~ 1mM (B), on glassy carbon electrode (ϕ = 3 mm), in acetonitrile containing *n*- Bu_4NPF_6 0.1 M, at a scan rate of 0.1 Vs^{-1}.

X-ray diffraction data were measured using an Agilent Xcalibur Atlas Gemini diffractometer using graphite-monochromated Mo-Kα radiation and ω scans at 130 K. Analytical numeric absorption correction using a multifaceted crystal was applied, a summary for data collection and refinements is given in Table 1. The structure was solved using direct methods, using SHELXS- 2012 and the refinement (based on F2 of all data) was performed by full-matrix least-squares techniques with SHELXL-2014.24. The perchlorate anions, two phenyl rings (C21→C26 and C27→C32), coordinated and uncoordinated solvent molecules, exhibit orientational and/or statistical disorder which was modeled (mainly) over two positions. All disordered atoms (except the solvent methanol molecule C49–O22, which turn to be NPD and was refined isotopically) were refined with restraints (SIMU and DELU) on

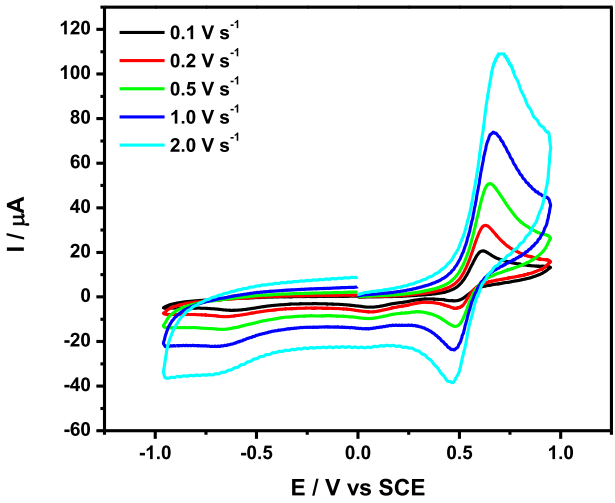

Fig. 10. Cyclic voltammetry at different scan rates for **3**—1 mM, on glassy carbon electrode ($\phi = 3$ mm), in acetonitrile containing *n*-Bu_4NPF_6 0.1 M.

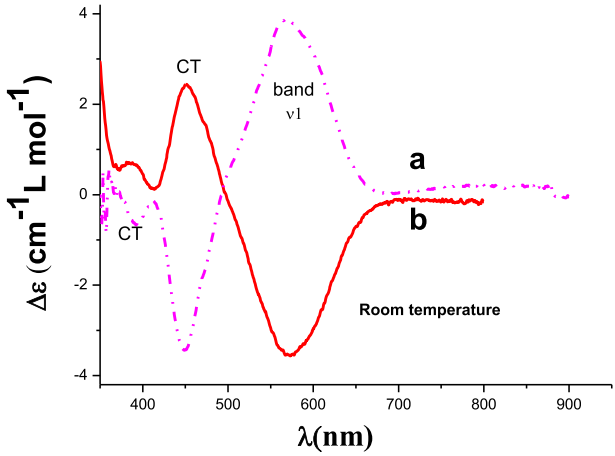

Fig. 11. CD spectra for the manganese polymeric compounds. **a**. *[Mn$_2$(S,S(+)Hcpse)$_4$(NaClO$_4$)$_2$(NaOH)(CH$_3$OH)]$_n$·[(C$_2$H$_6$O)$_2$]$_n$·[(CH$_4$O)$_2$]$_n$* and **b**. *[Mn$_2$(R,R(−)Hcpse)$_4$(NaClO$_4$)$_2$(NaOH)(CH$_3$OH)]$_n$·[(C$_2$H$_6$O)$_2$]$_n$·[(CH$_4$O)$_2$]$_n$*.

anisotropic displacement parameters and the bond geometries of the disordered groups were constrained or restrained to be similar with the AFIX or SADI commands of SHELXL. In addition, the contribution of a smeared un-coordinated solvent was "squeezed" using the PLATON program. IR spectra in the range 4000–400 cm^{-1} were recorded on a Nicolet FT-IR 740 spectrophotometer using KBr pellets. Electronic spectra (diffuse reflectance) were measured on a Cary 5E Uv–Vis–NIR spectrophometer in the range 250–2500 nm (40000 - 5000 cm^{-1}). Elemental analyses were performed on a Fisons EA 1108 elemental analyser. Circular dichroism measurements were performed on a JASCO J815 spectrophotometer. Magnetic susceptibility measurements were carried out with a pendulum-type magnetometer (MANICS DSM8) equipped with an Oxford CF 1200 S helium continuous-flow cryostat working in the temperature range 300–400 K, in a magnetic field of 3 Oe. Powder diffraction was recorded on SIEMENS D500, graphite-monochromated Cu-Kα ($\lambda = 1.5406$ Å) radiation at 293 K, CT: 0.6 s, SS: 0.020 dg, WL = 1.5406 Å. The chemical analysis was obtained using X-ray photoelectron spectroscopy (XPS). This was performed using a VG Microtech ESCA2000 Multilab UHV system, with

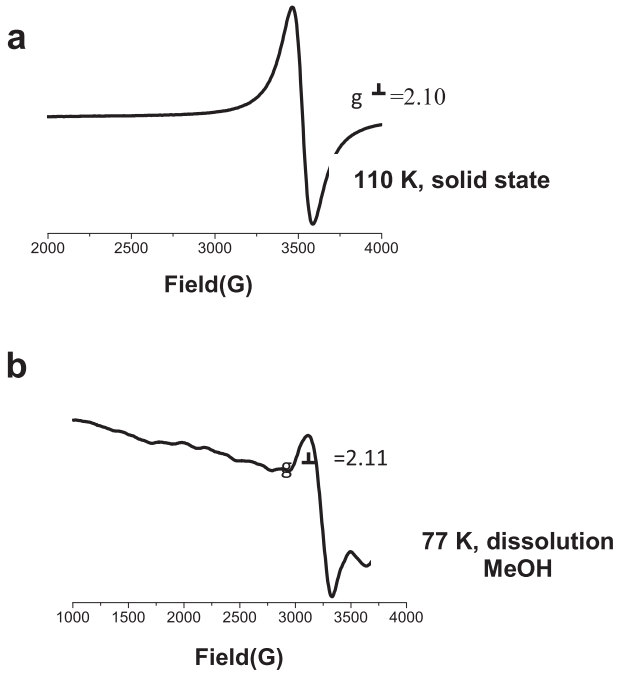

Fig. 12. X-band spectra of *[Mn2(S,S(+)Hcpse)4(NaClO4)2(NaOH)(CH3OH)]n·[(C2H6O)2]n·[(CH4O)2]n* **a**. 110 K, solid state; **b**. 77 K, dissolution, 2.03mM.

an Al K_α x-ray source ($h\nu = 1486.6$ eV), and a CLAM4 MCD analyser. XPS spectrum was obtained at 55° from the normal surface in the constant pass analyser energy mode (CAE), $E_0 = 50$ and 20 eV for survey and high resolution narrow scan. Peak positions were referenced to the background silver $3d_{5/2}$ core level at 368.20 eV, having a FWHM of 1.00 eV, Au $4f_{7/2}$ in 84.00 eV and C 1s hydrocarbon groups in 285.00 eV central peak position. The XPS spectra were fitted with the program SDP v 4.1. Electrochemical experiments were carried out in a conventional three-electrode cell, with a glassy carbon disc ($\phi = 3$ mm), a platinum mesh and a saturated calomel electrode (SCE) as working, auxiliary and reference electrodes, respectively. The supporting electrolyte was *n*-tetrabutylammonium hexafluorophosphate (*n*-Bu_4NPF_6) 0.1 M.

2. Experimental design, materials, and methods

2.1. Materials

The metal salt $Mn(CH_3COO)_2 \cdot 4H_2O$, $NaClO_4$, NaOH, and methanol (J.T. Baker) were used without further purification. The synthesis of the ligands *N*-[2-hydroxy-1(*R*)-methyl-2(*R*)-phenylethyl]-*N*-methylglycine *(R,R(−)*H_2cpse and *N*-[2-hydroxy-1(*S*)-methyl-2(*S*)-phenylethyl]-*N*-methylglycine (*S,S* (+)H_2cpse) was carried out as previously described; [8].

2.2. Synthesis

2.2.1. Synthesis of compound $[Mn_2(S,S(-)Hcpse)_4(NaClO_4)_2(NaOH)(CH_4O)]_n \cdot [(C_2H_6O)_2]_n \cdot [(CH_4O)_2]_n$

S,S (+)H_2cpse (479 mg, 2.14 mmol) in methanol (15 mL) was mixed with $Mn(CH_3COO)_2 \cdot 4H_2O$ (265 mg, 0.108 mmol) and stirred during 15 minutes. Then, $NaClO_4$ (13 mg, 0.109 mmol) was added to the mixture at basic pH and stirred again during 15 minutes. After two weeks brown needles, suitable for

X-ray diffraction analysis, were obtained (Yield 84% (261 mg)). The compound showed to be hygroscopic. Calculated analysed (Anal. Calcd) for $Mn_2C_{54}H_{91}Cl_2N_4Na_3O_{28}$: C%, 42.90; H%, 6.21; N%, 3.71. Exp.: C%, 43.15%; H% 5.77; N% 3.84. IR (KBrν/cm^{-1}): 1569 (ν_{as} COO^-) and 1443 ($\nu_s COO^-$), $\Delta\nu_{(as\text{-}s)} = 126$ cm-1. MS: *m*/*z* [M]+, 99(87), 305(57), 146(38), 575(32), 875(30), 1179(13), 1098(12).

2.2.2. Synthesis of compound [Mn_2(R,R(−)Hcpse)$_4$($NaClO_4$)$_2$(NaOH)(CH_4O)]$_n$·[(C_2H_6O)$_2$]$_n$ [(CH_4O)$_2$]$_n$

To a solution of R,R (−)H_2cpse (481 mg, 2.16 mmol) in methanol (15 mL), $Mn(CH_3COO)_2 \cdot 4H_2O$ (269 mg, 1.109 mmol) was added. The mixture was stirred for 15 minutes. After two weeks there was obtained a brown microcrystalline compound, not suitable for monocrystal X-ray diffraction analysis. Yield 87% (283 mg). The compound showed to be hygroscopic. Anal. Calcd for $Mn_2C_{54}.H_{89}Cl_2N_4Na_3O_{27}$: C%, 43.42; H%, 6.14; N%, 3.75. Exp.: C%, 43.85%; H%,5.93; N%, 3.75. IR (KBrν/cm^{-1}): 1569 (ν_{as} COO^-) and 1443 (ν_s COO^-) $\Delta\nu_{(as\text{-}s)} = 126$ cm-1. These methodology has been used by Barba- Behrens and et-al for tridentate ligands derivate of *N*- Acetyl pseudoephedrine, [8–10].

Acknowledgments

The authors of the paper thank to Universidad Santiago de Cali GRANTS DGI 63661 and Universidad Nacional Autónoma de México.

Conflict of Interest

The authors declare that they have no known competing financial interests or personal relationships that could have appeared to influence the work reported in this paper.

References

[1] J. Whittaker, Arch. Biochem. Biophys. 525 (2012) 111–120. https://doi:10.1016/j.abb.2011.12.008.
[2] S. Mishra, J. Imlay, Arch. Biochem. Biophys. 525 (2012) 145–160, https://doi.org/10.1016/j.abb.2012.04.014.
[3] A. Prieto, C.R.S.C. Rovira, Theoretical and computational chemistry series, 2017, pp. 453–480. https://doi:10.1039/9781782626831-00453.
[4] A. Moreira- Meireles, A. Almeida- Lage, J. Martins, M. Neres da Silva, M. Fagundes, D. Martins, Environ. Res. 177 (2019) 108615, https://doi.org/10.1016/j.envres.2019.108615.
[5] G. Wang, D.Y. Zhao, F.Y. Kou, Q. Ouyang, J.Y. Chen, Z.Q. Fang, Chem. Eng. J. 351 (2018) 747–755. https://doi: 0.1016/j.cej.2018.06.033.
[6] R.A. Sheldon, in: R.A. Sheldon (Ed.), Metalloporphyrins in Catalytic Oxidations, Marcel Dekker, Inc., New York, 1994, pp. 1–27.
[7] V. Bagchi, D. Bandyopadhyay, Inorg. Chim. Acta 363 (2010) 2786–2790. https://doi:10.1016/j.ica.2010.03.071.
[8] Y. Ávila-Torres, L. Huerta, N. Barba-Behrens, J. Chem. 370637 (2013) 1–9, https://doi.org/10.1155/2013/370637.
[9] I. Valencia, Y. Ávila-Torres, N. Barba-Behrens, Garzón. I. Journal of Molecular Structure. 1085 (2015) 52–62, https://doi.org/10.1016/j.molstruc.2014.12.061.
[10] Y. Ávila-Torres, H. López-Sandoval, E. Mijangos, L. Quintanar, E.E. Rodríguez, A. Flores-Parra, Vicente R. Contreras, G.L.A. Rikken, Barba-Behrens. N. Polyhedron. 51 (2013) 298–306, https://doi.org/10.1016/j.molstruc.2014.08.020.